Aeolian Research 20 (2016) 157–168

Contents lists available at ScienceDirect

Aeolian Research

journal homepage: www.elsevier.com/locate/aeolia

Validation of SWEEP for creep, saltation, and suspension in a desert–oasis ecotone

H. Pi [a], B. Sharratt [b,*], G. Feng [a,1], J. Lei [a], X. Li [a], Z. Zheng [a]

[a] State Key Laboratory of Desert and Oasis Ecology, Xinjiang Institute of Ecology and Geography, Chinese Academy of Sciences, Urumqi, Xinjiang 830011, China
[b] USDA-ARS, 215 Johnson Hall, Pullman, WA 99164, USA

ARTICLE INFO

Article history:
Received 9 November 2015
Accepted 28 January 2016
Available online 10 February 2016

Keywords:
Creep
Saltation
Suspension
SWEEP
WEPS
Wind erosion

ABSTRACT

Wind erosion in the desert–oasis ecotone can accelerate desertification, but little is known about the susceptibility of the ecotone to wind erosion in the Tarim Basin despite being a major source of windblown dust in China. The objective of this study was to test the performance of the Single-event Wind Erosion Evaluation Program (SWEEP) in simulating soil loss as creep, saltation, and suspension in a desert–oasis ecotone. Creep, saltation, and suspension were measured and simulated in a desert–oasis ecotone of the Tarim Basin during discrete periods of high winds in spring 2012 and 2013. The model appeared to adequately simulate total soil loss (ranged from 23 to 2272 g m^{-2} across sample periods) according to the high index of agreement ($d = 0.76$). The adequate agreement of the SWEEP in simulating total soil loss was due to the good performance of the model ($d = 0.71$) in simulating creep plus saltation. The SWEEP model, however, inadequately simulated suspension based upon a low d ($\leqslant 0.43$). The slope estimates of the regression between simulated and measured suspension and difference of mean suggested that the SWEEP underestimated suspension. The adequate simulation of creep plus saltation thus provides reasonable estimates of total soil loss using SWEEP in a desert–oasis environment.

Published by Elsevier B.V.

1. Introduction

The desert–oasis ecotone is a dynamic and interactive zone where interchange of energy and mass occurs between the desert and oasis ecosystems. Oasis evolution, which consists of two opposing processes of oasification and desertification, occurs in this zone and thus plays a prominent role of ensuring oasis ecological security and maintaining oasis ecological stability. Wind erosion in the desert–oasis ecotone can accelerate desertification and is an important indicator of oasis ecological security (Su et al., 2007). Therefore, assessing the susceptibility of the landscape to wind erosion is important for protecting this ecological zone from desertification caused by anthropogenic activities as well as natural variations in climate.

The Tarim Basin is a 1 million km^2 endorheic basin that lies within Xinjiang Province of northwestern China. The region is surrounded by the Kunlun mountain range to the south, Pamir mountain range to the west, and Tian Shan mountain range to the north. These mountains, with elevations over 7000 m, greatly influence the climate across the region. Atmospheric moisture, transported into the region by prevailing westerly winds, is typically intercepted by these mountains. The lack of moisture transported into the Tarim Basin results in an arid environment.

Wind erosion threatens ecosystem stability in the Tarim Basin. Dust storms contribute to poor air quality and visibility in the Tarim Basin and many other arid and semiarid regions throughout the world (Chan et al., 2005; Sharratt and Lauer, 2006). Wind erosion models aid in predicting the occurrence of erosion events and developing management practices for controlling wind erosion and thereby improving air quality and health of ecosystems. The Wind Erosion Prediction System (WEPS) was developed by the USDA Agricultural Research Service (Hagen, 1991; Wagner, 2013) as a tool to simulate soil and PM10 (particulate matter $\leqslant 10$ μm in aerodynamic diameter) loss from agricultural landscapes. Since the inception of WEPS, the model has rarely been validated for land use types other than agriculture and in arid environments. For example, Visser et al. (2005) found good agreement between measured and simulated wind erosion in the Sahel although their observations were restricted to agricultural lands. Maurer and Gerke (2011) validated WEPS on an artificial sandy catchment devoid of vegetation in the mining district of southern Germany. Their validation, however, relied on qualitative measures of wind

* Corresponding author at: USDA-ARS, 215 Johnson Hall, Pullman, WA 99164-6421, USA. Tel.: +1 509 335 2724.
E-mail address: Brenton.sharratt@ars.usda.gov (B. Sharratt).
[1] Current address: USDA-ARS, 810 Highway 12 East, Mississippi State, MS 39762, USA.

http://dx.doi.org/10.1016/j.aeolia.2016.01.006
1875-9637/Published by Elsevier B.V.

erosion obtained from aerial imagery. Adapting WEPS to land use types other than agriculture is important for model improvement and application to a diversity of land managers (Van Donk et al., 2003). The validation of WEPS and SWEEP for predicting wind erosion in the desert–oasis ecotone will aid in improving model performance and advance progress in promoting ecosystem stability in the region.

Wind erosion processes involve transport of sediment by creep, saltation and suspension. Aggregates or particles 0.1–2.0 mm in diameter generally creep and saltate along the surface while aggregates or particles <0.1 mm in diameter are suspended above the surface (Hagen et al., 1999). This designation of aggregate or particle size is used by the WEPS in simulating transport processes. Some variation exists in differentiating transport processes by aggregate or particle size because particle shape and density and shear stress influence particle motion. In fact, observations by Mikami et al. (2005) and Sharratt (2011) suggest that aggregates or particles as small as 0.04 mm can saltate along the surface. The energy contained in particles saltating along the surface can result in extensive damage to plants. Indeed, sandblasting can adversely affect plant development and productivity (Armbrust, 1984). The suspension component is derived from direct emission of fine particles on the surface or emission of particles that are abraded or broken down from larger particles resting on the surface or being transported by creep and saltation (Hagen, 2004a). Of importance to air quality is the transport of suspension and more importantly, PM10, which is regulated by many nations throughout the world (Sharratt and Edgar, 2011).

Few scientists have measured the size distribution of windblown sediment for separating creep, saltation, and suspension components of wind erosion. Nevertheless, separating windblown sediment into creep-size, saltation-size, and suspension-size components is critical for validating some wind erosion models and furthering our understanding of transport processes (Hagen et al., 2010). Sharratt et al. (2007) found that suspension was the dominate process of wind erosion of loessial soils in the Columbia Plateau of the Pacific Northwest United States. They found 94% of sediment in transport was by suspension whereas 2% and 4% of sediment in transport was by respectively creep and saltation. Chepil (1945) observed that soil type influenced the proportion of particles transported by creep, saltation and suspension. Although the predominate mode of transport was by saltation for a sand, sandy loam, loam, and clay, transport by creep (ranging from 7% to 25% of the mass flux) appeared to be more important with an increase in sand content of the soil. For aeolian sands, saltation dominates the wind erosion process. Tchakerian (1999) reported that saltation accounted for 80% of the transport load while suspension comprised only 5% of the transport load. Saltation is important in promoting and sustaining mass transport because saltating particles impacting a surface can overcome shear and interparticle forces and thus mobilize particles of varying size. Transport by creep has been found to account for 10 (Namikas, 2003), 25 (Willetts and Rice, 1985), and up to 40% of total sand flux (Rotnicka, 2013). The mass proportion of particles transported by creep decreases with an increase in particle size (Dong et al., 2002) and friction velocity (Wang and Zheng, 2004).

The WEPS erosion submodel, or the Single-event Wind Erosion Evaluation Program (SWEEP), has been validated for total soil loss and soil discharge from agricultural fields around the world (Buschiazzo and Zobeck, 2008; Feng and Sharratt, 2009; Funk et al., 2004). There is relatively little known regarding the performance of the SWEEP applied to other environments. We are not aware of any studies that have tested the performance of the SWEEP in simulating erosion in a desert–oasis ecotone or the relative and separate contributions of creep, saltation, and suspension to the total sediment load. Accurate simulation of these components to the total sediment load is vital for developing wind erosion control strategies that foster ecosystem stability. Therefore, the focus of this study was to examine the performance of the SWEEP in simulating creep, saltation, and suspension processes within a desert–oasis ecotone.

2. Materials and methods

The performance of the SWEEP in simulating creep, saltation, and suspension processes was validated at a desert–oasis ecotone site in Xinjiang Province, China (Fig. 1) in 2012 and 2013. The desert–oasis ecotone site was located about 10 km south of Alaer City (40°27′N, 81°19′E, elevation of 992 m) near the confluence of the Aksu, Hotan, and Yarkand Rivers; these rivers join to form the Tarim River in the northwest part of the Tarim Basin. The desert–oasis ecotone is characterized by relatively level topography and bordered by irrigated land along the rivers and tributaries and desert. Shifting transverse sand dunes, oriented northeast-southwest, are also interspersed across the ecotone. The average annual precipitation of this region is 53 mm and the average annual temperature is 11.3 °C.

2.1. Measured soil loss

Creep and Big Spring Number Eight (BSNE) sediment collectors (Custom Products and Consulting, Big Spring, TX) were used to measure horizontal soil flux at the experimental plot located about 5 km south of the Tarim River (Fig. 2). The soil type at the experimental plot was aeolian sand with vegetation sparsely distributed across the plot and consisting of Saltbush (*Atriplex polycarpa* L.) and Manaplant Alhagi (*Alhagi sparsifolia* L.). The vegetation provided <5% cover (Table 1) and trapped blowing sand to form a small shrub-coppice dune (<0.25 m high) around the vegetation. Sediment collectors were positioned in the plot to provide a minimum of 0.3 km of fetch in the direction of the prevailing winds (NW). An ephemeral tributary (30 m wide and 1 m deep) and paved road (10 m wide and 1 m of relief), with intervening vegetation consisting of Saltcedar (*Tamarix ramosissima* L.) and Manaplant Alhagi, minimized the influx of soil along the windward side of the experimental plot. The height of Saltcedar and Manaplant Alhagi were respectively 2 and 0.1 m; this vegetation resulted in a biomass cover of 50% between the tributary and road. The paved road and tributary respectively traversed the landscape in a NE–SW and ENE–WSW direction for several kilometers at the ecotone site. Irrigated red date trees occupied the land to the NW of the tributary. Although only visually substantiated during one erosion event, these barriers were assumed to provide a "zero soil flux boundary" during prevailing NW winds in this study. The authors witnessed no sediment blowing across the road even though sediment was blowing across the experimental plot during one high wind event (17–19 April 2013). Transverse and fixed shrub-coppice dunes were located along the SE border of the plot (Fig. 2). The transverse dunes were oriented NE–SW, had 1 m of relief, and were 1 km long and 7 m wide. Vegetation growing between the two transverse dunes (the dunes were 30 m apart) consisted of Saltcedar and Manaplant Alhagi. The height of the Saltcedar and Manaplant Alhagi were respectively 2 and 0.2 m and biomass cover was 90%. The prolific vegetation growing between the two dunes was due to higher moisture in the interdune area (Wang et al., 2004). The fixed or stable dunes abutted the transverse dunes and were 2 m in height, 10 m wide, and 30 m long. The transverse dunes and intervening vegetation were assumed to provide a "zero soil flux boundary" along the SE border of the experimental plot when winds were from the SE.

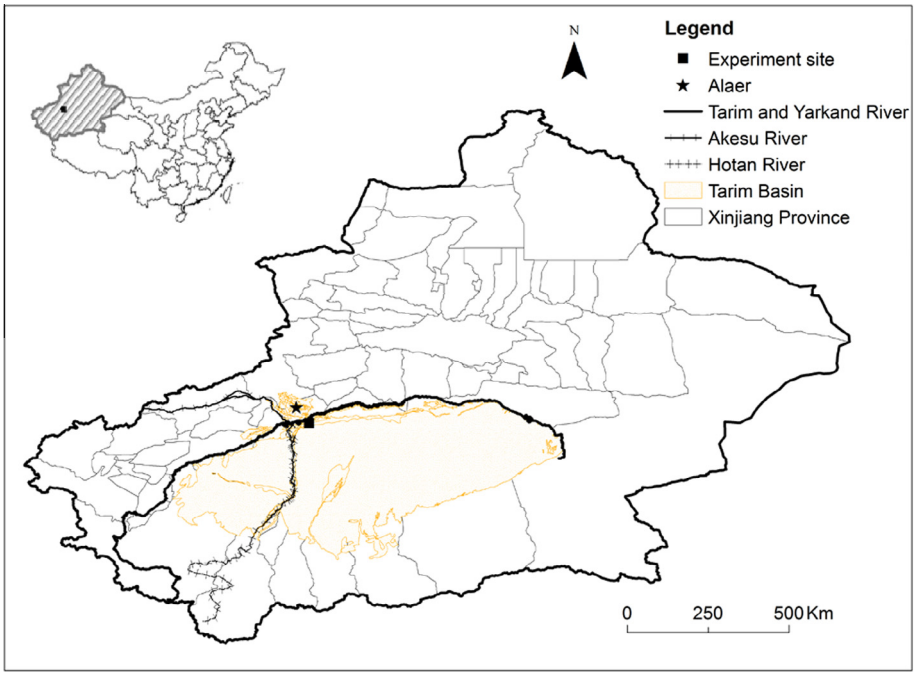

Fig. 1. Location of the experiment site in the Tarim Basin, China. The small map depicts Xinjiang Province in China while the large map is of Xinjiang Province. The Aksu, Hotan, and Yarkand Rivers join to form the Tarim River.

Creep and BSNE collectors were positioned to avoid obstructions to airflow caused by the small shrub-coppice dunes and sparse vegetation within the plot. Creep collectors captured sediment to a height of 0.025 m while BSNE airborne collectors were positioned 0.1, 0.2, 0.5, 1.0, 1.5 and 2.0 m above the soil surface. Three groups of collectors, with each group comprising one creep and six BSNE collectors, were spaced 3 m apart along a line perpendicular to the prevailing wind and near a meteorological tower (Fig. 2).

Sediment in the collectors was retrieved periodically due to the remoteness of the site and infrequency of high winds sufficient to cause wind erosion. Our intent was to retrieve sediment from the collectors immediately after a singular or series of high wind events having predominately unidirectional winds. Sediment from the collectors was placed in plastic bags and transported to the laboratory where the samples were air-dried, weighed, and sieved. The equation of Zobeck and Fryrear (1986) was used to describe the vertical distribution of sediment captured by BSNE collectors, which is

$$q = \alpha z^{-\beta} \quad (1)$$

where q is sediment catch (kg m^{-2}), z is height (m) of the opening of the BSNE collector above the soil surface and α and β are fitted parameters. Eq. (1) was integrated from 0.025 to 2 m using the power method to obtain total BSNE horizontal soil flux (kg m^{-1}) for the sample period.

The catch efficiency of the BSNE collector is >90% for sand, but is influenced by both particle size and wind speed (Fryrear, 1986; Mendez et al., 2011; Sharratt et al., 2007). Goossens et al. (2000) found the efficiency of the BSNE collector was about 100% for sand having a geometric diameter similar to that at our field site (see below). Catch efficiency of the BNSE for suspension-size particles varies widely, from 60% to 165% (Fryrear, 1986; Sharratt and Feng, 2009). The lack of consensus regarding catch efficiency of the BSNE collector creates uncertainty in adjusting suspension based upon any inefficiency in the collector. Therefore, no adjustment was made to account for any inefficiency of the collector in this study. Eq. (1) was integrated to 2 m height because sediment catch approached zero and the integrated flux for all high-wind events approached maximum value at this height. Total horizontal soil flux represents the sum of creep flux and total BSNE horizontal soil flux. Loss of soil from the experimental plot was calculated as total horizontal soil flux divided by the distance between the collectors and "zero soil flux boundary" (road or transverse sand dune) in the direction of the prevailing wind.

Sediment trapped by the creep and BSNE collectors was air-dried and then hand sieved through screens having 2, 0.84, and 0.1 mm openings to determine the proportion of creep-size, saltation-size, and suspension-size particles in each collector. For the purpose of this study, the creep-size, saltation-size and suspension-size fractions were respectively comprised of particles 2–0.84, 0.84–0.1, and <0.1 mm particles. These size fractions are specifically used in SWEEP to represent the different modes of sediment transport. Variation in particle size representing modes of transport, however, exists in the literature. For example, creep-size has been designated as particles with diameters $\geqslant$1 (Fryrear et al., 1991), $\geqslant$0.8 (Hagen, 2010), and $\geqslant$0.5 mm (Lyles, 1977). Particles with diameters of 0.1 mm have even been shown to creep along the surface (Zhang et al., 2014). Similarly, suspension-size has been designated as particles with diameters <0.1 mm (Fryrear et al., 1991) and <0.07 mm (Shao, 2000).

Horizontal flux of creep-size, saltation-size, and suspension-size particles was respectively assessed from the proportion of particles 2–0.84, 0.84–0.1, and <0.1 mm in diameter in each creep and BSNE collector and using Eq. (1) to determine total BSNE horizontal flux for creep-size, saltation-size, and suspension-size particles. Total horizontal flux of creep-size, saltation-size, or suspension-size particles is the sum of the flux from both creep and BNSE collectors. Loss of creep-size, saltation-size, and suspension-size particles from the experimental plot was calculated as total horizontal flux divided by the distance between the collectors and "zero soil flux boundary".

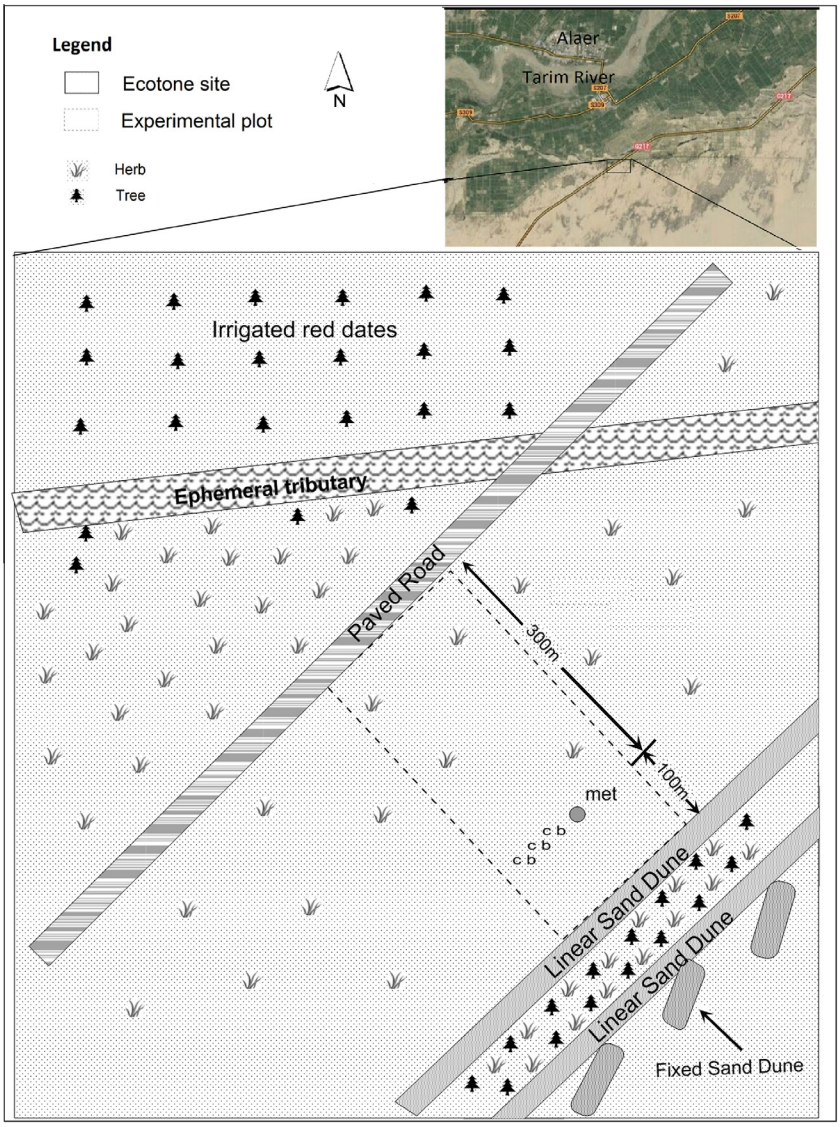

Fig. 2. Location of instrumentation in the experimental plot with symbols representing placement of BSNE (b) and creep (c) collectors and meteorological (met) station.

2.2. SWEEP

The WEPS is a process-based model that simulates weather, field conditions, and creep, saltation, suspension, and PM10 emission in response to wind speed, wind direction, field orientation and surface conditions on a subhourly basis (Hagen, 1991, 2004b; Hagen et al., 1995, 1999). The erosion submodel of WEPS, or SWEEP, can be used to simulate erosion across a gridded field during single high wind events (Tatarko, 2008). The grid size used in our study was 20 × 20 m (default value in SWEEP). The model simulates soil discharge from each grid cell (Tatarko, 2008) based upon known vegetation characteristics, surface properties, and wind. In addition to simulating soil discharge, the model also subdivides soil discharge into three transport components that include creep/saltation, suspension, and PM10 emission (Hagen et al., 1995; Hagen, 1997). Creep and saltation are treated as a single transport component in the SWEEP even though the mode of transport that governs these processes are differentiated in the field by particles that respectively roll and bounce along the surface.

The SWEEP model was designed to simulate soil loss and soil deposition over a rectangular field. This study used a rectangular plot 200 m wide by 400 m long (Fig. 2). The width of the plot, however, varied with wind direction (discussed later in paper). Input parameters representing surface characteristics and properties required by SWEEP, which were measured before and after development of leaves on vegetation in the experimental plot in 2013, are listed in Table 1. The parameters in Table 1 were regarded as representative of surface characteristics in 2012 because of the natural and stable environment. Wind speed data (see below) averaged over 15 min intervals were used for the simulations. The SWEEP is designed for simulating erosion for a single day, thus erosion events that spanned multiple days were separated into singular days for the simulation.

2.2.1. Vegetation parameters

The SWEEP model was developed to predict soil loss by wind from agricultural crop land. Unlike crop land that is managed to optimize the spatial architecture of plants for achieving maximum yield, the vegetation at our site has an irregular distribution across the landscape. Therefore, we assumed no crop row spacing and seed placement to portray a random distribution of vegetation in SWEEP. The vegetation at our site remained dormant over winter until early May at which time leaves began to emerge on the stems. We measured crop parameters within four 4 × 10 m sample areas

Table 1
Input parameters required by SWEEP for model validation. Parameters were measured before and after leafing of vegetation in spring 2013 in a desert–oasis ecotone.

Crop	Before May	After May
Residue average height (m)	0.63	0
Residue stem area index ($m^2\ m^{-2}$)	0.001	0
Residue leaf area index ($m^2\ m^{-2}$)	0	0
Residue flat cover ($m^2\ m^{-2}$)	0.039	0.039
Growing crop average height (m)	0	0.63
Growing crop stem area index ($m^2\ m^{-2}$)	0	0.001
Growing crop leaf area index ($m^2\ m^{-2}$)	0	0.001
Row spacing (m)	0	0
Seed placement	0	0
Soil		
Number of soil layers	1	1
Layer thickness (mm)	30	30
Bulk density ($Mg\ m^{-3}$)	1.58	1.58
Sand fraction (0.05–2.0 mm, $Mg\ Mg^{-1}$)	0.996	0.996
Very fine sand fraction (0.05–0.1 mm, $Mg\ Mg^{-1}$)	0.243	0.243
Silt fraction (0.002–0.05 mm, $Mg\ Mg^{-1}$)	0.004	0.004
Clay fraction (<0.002 mm, $Mg\ Mg^{-1}$)	0.0001	0.0001
Rock volume fraction ($m^3\ m^{-3}$)	0	0
Average aggregate density ($Mg\ m^{-3}$)	2.50	2.50
Average dry aggregate stability [ln(J kg^{-1})]	7.0	7.0
GMD of aggregate size (mm)	0.254	0.254
GSD of aggregate size ($mm\ mm^{-1}$)	2.748	2.748
Minimum aggregate size (mm)	0.05	0.05
Maximum aggregate size (mm)	1.0	1.0
Soil wilting point water content ($Mg\ Mg^{-1}$)	0.157	0.157
Surface crust fraction ($m^2\ m^{-2}$)	0	0
Surface crust thickness (mm)	0	0
Loose material on crust (plastic mulch)	0	0
Loose mass on crust ($kg\ m^{-2}$)	0	0
Crust density ($Mg\ m^{-3}$)	0	0
Crust stability [ln(J kg^{-1})]	0	0
Allmaras random roughness (mm)	1.0	1.0
Ridge height (mm)	0	0
Ridge spacing (mm)	0	0
Ridge width (mm)	0	0
Ridge orientation (deg)	0	0
Snow depth (mm)	0	0
Hourly surface water content ($gg^{-1} \times 100$)	0	0
Weather		
Wind direction (deg)	Table II	
Wind speed	Fig. 3	

in proximity to our instruments. Stem area index was determined by measuring the diameter (4 mm), height (112 mm), and population of stem elements (1.82 stems m^{-2}). Leaf area index was assessed by measuring the width and length of 10 representative leaves and counting the number of leaves on all stems. The height of residue and growing crop was measured by a ruler.

2.2.2. Surface parameters

The SWEEP requires information about aggregate size distribution, aggregate stability and density, primary particle size distribution, and surface roughness characteristics (Table 1). Since aeolian sand lacks fine particles and microbial activity important in the formation of aggregates, the soil was largely composed of single sand grains. Soil samples (about 0.5 kg taken from the upper 10 mm of the profile) at 10 locations in the experimental plot were placed on trays and transported in cushioned boxes to the laboratory for analysis. Samples were air-dried for >48 h prior to analysis. Aggregate size distribution was determined by sieving samples using a horizontal sieve shaker (Model, ZBSX 92A, Shanghai zheTiMachinery Manufacturing Company, China) that oscillated a stack of nine sieves (10, 5, 2, 0.84, 0.50, 0.25, 0.10, and 0.075 mm) at a frequency of 124 times per minute for 3 min. Soil primary particle size distribution was determined by agitating and dispersing the soil with sodium hexametaphosphate prior to using a Mastersizer laser diffraction instrument (Malvern Instruments, Worcestershire, UK) to measure particle size distribution (see Table 1).

Aggregate size distribution is used to define transport processes in SWEEP. The SWEEP defines aggregate size distribution based upon the aggregate geometric mean diameter (GMD) and standard deviation (GSD) and maximum and minimum aggregate sizes of the log-normal distribution. The GMD and GSD were determined by fitting the measured mass percentage of different aggregate sizes, obtained using the horizontal sieve apparatus, to a log-normal function (Gardner, 1956). The GMD and GSD of the aggregate size distribution were respectively 0.254 mm and 2.748 mm mm^{-1}. The horizontal sieve apparatus has an aggressive sieve action that could potentially cause undesirable aggregate breakdown compared to a rotary sieve apparatus, which is typically used to assess aggregate size distribution. Maximum and minimum aggregate sizes were respectively <0.5 and <0.075 mm according to the measured aggregate size distribution and assumed to be 0.4 and 0.05 mm based upon the largest and smallest primary particle size found using the Mastersizer laser diffraction instrument. However, the maximum aggregate size was designated as 1.0 mm as this is the minimum value allowed by the SWEEP model (Tatarko, 2008). The maximum and minimum aggregate sizes of 1.0 and 0.05 mm also represent the range in grain sizes of aeolian sands in the Tarim Basin (Honda and Shimizu, 1998; Wang et al., 2003). We also simulated wind erosion using a maximum and minimum aggregate size of respectively 1.54 and 0.01 mm, which are estimates derived by the SWEEP based upon the GMD and GSD (Tatarko, 2008). Soil particles from our experimental plot were assumed to be very stable, thus we used the maximum aggregate density and stability allowed by the SWEEP model. The GMD and GSD of the soil primary particle size distribution were respectively 0.230 mm and 2.50 mm mm^{-1}. Since the GMD and GSD of the aggregate size and primary particle size distributions were similar, we conclude that little aggregation existed in the upper 10 mm of the profile.

Soil physical properties were measured at three locations within the experimental plot. Soil bulk density was determined by extracting 0.07 m diameter by 0.03 m long samples from the soil profile and then drying at 105 °C prior to measuring the soil dry weight (bulk density). No crust was observed on the surface during our study. Random roughness was measured using a pin-type profile meter (Allmaras et al., 1966) which was comprised of a rigid frame and pins that moved vertically through holes in the frame. The frame was mounted above the soil surface after which the pins, spaced 25 mm apart across the 1 m frame, were lowered to the surface. Random roughness was then determined as the standard deviation among pin heights after correcting for slope (Currence and Lovely, 1970). The surface had little random roughness as a consequence of the surface being comprised of single sand grains. Although random roughness was <1 mm, we report a value of 1 mm in Table 1 as this is the minimum value allowed by the SWEEP model. Soil water content was determined by extracting 0.07 m by 0.01 m samples from the soil profile and determining the reduction in weight of samples before and after drying at 105 °C. Water content varied from 0.0012 to 0.0019 g g^{-1} during the course of the experiment. Surface water content can affect wind erosion by influencing the threshold friction velocity (Tatarko, 2008). Threshold friction velocity increases with surface water content in SWEEP according to:

$$UW^*t = UB^*t + 0.48\frac{HRO_{wc}}{HR15_{wc}} \quad (2)$$

where UW*t is threshold velocity of a wet surface, UB*t is the threshold velocity of a bare and dry surface, HRO_{wc} is surface water content (g g^{-1}), and $HR15_{wc}$ is surface water content at 1.5 MP_a

($g\,g^{-1}$) (Tatarko, 2010). An increase in threshold friction velocity occurs only when $\frac{HRO_{wc}}{HR15_{wc}}$ is > 0.2 (Saleh and Fryrear, 1995). Based upon a measured $HR15_{wc}$ of 0.157 $g\,g^{-1}$ and HRO_{wc} of <0.002 $g\,g^{-1}$, surface water content did not influence threshold friction velocity in our study. Sharratt et al. (2013) found that soil water content will influence threshold friction velocity only when gravimetric water content exceeds 6%. Since surface water content had no influence on threshold friction velocity and thus wind erosion in our study, soil water content was set to zero (Table 1).

2.3. Weather

An automated meteorological station was established at the experimental site to measure wind speed and direction, precipitation, solar radiation, and atmospheric temperature and relative humidity. Anemometers were placed at heights of 0.1, 0.5, 1, and 10 m above the soil surface. Micrometeorological sensors were monitored every 10 s and data recorded every 15 min by a datalogger (Model 10X, Campbell Scientific Inc., Logan, Utah).

High wind events were defined by threshold wind velocities of $\geqslant 4\ m\,s^{-1}$ at a height of 1 m in our study. This threshold velocity was determined from the known soil particle size and roughness of the surface. Bagnold (1941) found that threshold velocity is related to particle size according to:

$$u_{*t} = A\sqrt{\frac{(\alpha-\rho)gd}{\rho}} \tag{3}$$

where u_{*t} is threshold friction velocity ($m\,s^{-1}$), A is an empirical coefficient of turbulence (approximately 0.1), α is particle density ($g\,m^{-3}$), ρ is air density ($g\,m^{-3}$), g is acceleration due to gravity ($m\,s^{-2}$), and d is particle diameter (m). Eq. (3) is valid for particles >0.1 mm in diameter according to Shao and Lu (2000). Based upon this equation, the threshold velocity of 0.25 mm diameter soil particles (mean particle diameter reported in Table 1) was 0.23 $m\,s^{-1}$. Surface aerodynamic roughness influences wind speed within the inertial sublayer according to the log wind speed profile:

$$u_z = \frac{u*}{k}\ln\frac{z}{z_o} \tag{4}$$

where u_z is wind speed ($m\,s^{-1}$) at height z (m), k is von Karman's constant (0.4), and z_o is surface aerodynamic roughness (m). For an observed aerodynamic roughness of about 1 mm during high winds at our experimental site (Li et al., 2015), a threshold velocity of about 4 $m\,s^{-1}$ was obtained at a height of 1 m.

2.4. Statistical analysis

Paired-samples t-test, regression analysis, model performance index of agreement (d), modeling efficiency (EF), mean, and root mean square error (RMSE) were used to compare measured soil loss and soil loss simulated by the SWEEP. The d is used to appraise model performance (Willmott, 1981) according to:

$$d = 1.0 - \frac{\sum_{i=1}^{N}(Pi-Oi)^2}{\sum_{i=1}^{N}(|Pi-\bar{O}|+|Oi-\bar{O}|)^2} \tag{5}$$

where Pi is the predicted value, Oi is the measured value, N is the number of comparisons, and $\bar{O}$ is the average measured value.

Modeling efficiency (Loague and Green, 1991) and RMSE are described by:

$$EF = \frac{\sum_{i=1}^{N}(Oi-\bar{O})^2 - \sum_{i=1}^{N}(Pi-Oi)^2}{\sum_{i=1}^{N}(Oi-\bar{O})^2} \tag{6}$$

$$RMSE = \sqrt{\frac{\sum_{i=0}^{N}(Pi-Oi)^2}{N}} \tag{7}$$

Ma et al. (2011) suggested that model performance is acceptable when d > 0.7. Modeling efficiency has a maximum value of 1.0 with EF values >0.7 indicating good agreement between measured and simulated soil loss. Lower RMSE values indicate better agreement between measured and simulated soil loss. The paired-Samples t-test was used to compare the difference between the measured and predicted soil loss. A probability level (P) of <0.05 indicated significant differences (McDonald, 2008) between the measured and simulated soil loss.

3. Result and discussion

Soil loss was assessed for 11 sampling periods over two years (Table 2). The highest wind speeds at our study site were recorded from 31 March to 11 April 2012 with maximum wind speeds of

Table 2
High wind event characteristics and total measured (meas) and simulated (sim) soil loss partitioned by creep plus saltation, and suspension in the desert–oasis ecotone during 2012 and 2013.

Year	Sampling period[1]	Events[2]	Hours[3]	Wind dir[4]	Wind speed[5]		EL[6]	Total soil loss		Creep plus saltation		Suspension		Sim maximum u_*	Sim u_{*t}
					Mean	Max		Meas	Sim	Meas	Sim	Meas	Sim		
				deg	$m\,s^{-1}$		m	$g\,m^{-2}$		$g\,m^{-2}$		$g\,m^{-2}$		$m\,s^{-1}$	
2012	31Mar–11Apr	5	16	161	5.3	8.3	111	2272	862	488	796	1784	66	0.44	0.28
	20–24Apr	3	7	277	4.9	5.7	381	99	15	18	13	81	2	0.30	0.28
	16–18May	2	8	297	4.8	6.6	315	597	173	108	157	489	16	0.35	0.28
2013	17–19Apr	2	6	255	5.0	6.4	600	26	16	7	14	19	2	0.34	0.28
	26–30Apr	3	8	155	4.4	5.6	106	161	5	50	4	111	1	0.29	0.28
	1–5May	3	20	63	4.6	6.6	324	216	151	58	139	158	12	0.35	0.28
	6–12May	3	13	124	5.3	7.2	102	448	226	80	106	368	120	0.38	0.28
	13–20May	5	21	245	4.7	7.2	877	23	10	4	9	19	1	0.38	0.28
	20–26May	6	30	140	5.2	6.9	100	387	129	90	113	297	16	0.36	0.28
	28May–2Jun	4	11	207	4.6	5.7	324	46	84	10	74	35	10	0.30	0.28
	3–16Jun	10	31	120	5.5	8.3	104	908	854	129	778	779	76	0.44	0.28

[1] Dates over which eroded soil was collected.
[2] Number of high wind events observed during the sampling period. A high wind event was defined by wind speeds that exceeded 4 $m\,s^{-1}$ at a height of 1 m.
[3] Number of hours during the sampling period for which wind speed exceeded 4 $m\,s^{-1}$ at a height of 1 m.
[4] Mean wind direction at 1 m height during the high wind events.
[5] Mean and maximum (max) wind speed at 1 m height during high wind events.
[6] EL is erosion length or distance from the sediment collectors to the non-erodible boundary in the direction of the prevailing wind.

8.29 m s^{-1} and winds in excess of 4 m s^{-1} at a height of 1 m for 16 h (Fig. 3). Information on wind speed during each sampling period including total hours of winds in excess of 4 m s^{-1}, mean wind direction and speed, and maximum wind speed is presented in Table 2.

3.1. Measured creep, saltation and suspension

Based upon data collected during the 11 sampling periods, soil loss ranged from 23 to 2272 g m^{-2} (Table 2). Soil loss was greatest during the 31 March–11 April 2012 sample period. Although maximum wind speed was similar for the 31 March–11 April 2012 and 3–16 June 2013 periods, the duration of winds in excess of 4 m s^{-1} for the 31 March–11 April 2012 sample period was half of the 3–16 June 2013 sample period. Winds in excess of 4 m s^{-1} were sustained for 16 h during the 31 March–11 April 2012 sampling period and 31 h for the 3–16 June 2013 period. However, the duration of winds in excess of 6 m s^{-1} for the 31 March–11 April 2012 sample period was more than the 3–16 June 2013 sample period. Winds in excess of 6 m s^{-1} were sustained for 13 h during the 31 March–11 April 2012 sampling period and 9 h for the 3–16 June 2013 period. Differences in wind direction (wind direction was 161° for the 31 March–11 April 2012 sample period and 120° for the 3–16 June 2013 sample period) and thus exposure of the sediment collectors to obstructions in airflow caused by shrub-coppice dunes and vegetation may have also influenced soil transport during these two sampling periods.

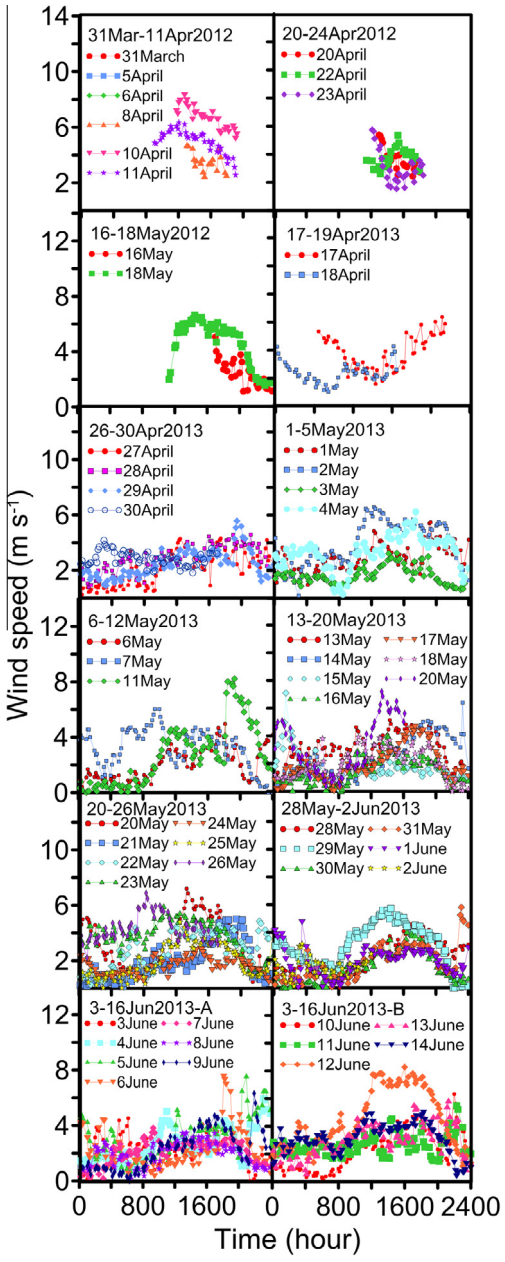

Fig. 3. Wind speed at a height of 1 m during high wind events in 2012 and 2013. For convenience, wind speed is portrayed as 15 min averages.

Winds at the experimental plot were not always from the NW or SE during high wind events (Table 2). Thus, the distance from the sediment collectors to the windward zero soil flux or non-erodible plot boundary will vary among high wind events due to differences in wind direction. The distance between the collectors and non-erodible boundary was respectively 300 and 100 m under prevailing NW and SE winds (Fig. 2); this distance was greater for more westerly or easterly winds (Table 2). The SWEEP model assumes a rectangular plot as shown in Fig. 2. The width of the plot was specified such that a non-erodible boundary was maintained along the NW and SE boundaries of the rectangular plot under more westerly or easterly winds. These non-erodible boundaries and specification of a rectangular plot allowed comparison of measured and simulated soil loss from the non-erodible boundary to the sediment collectors. Soil loss reported in Table 2 is based upon the distance between the collectors and non-erodible boundary in the direction of the prevailing wind. The width of the experimental plot used in SWEEP was therefore specified to maintain a non-erodible boundary at the windward border of the plot during a high wind event. The maximum width of the experimental plot to maintain a non-erodible boundary was 900 m; this plot width was required to determine measured and simulated soil loss for the 13–20 May 2013 high wind event. The landscape within the plot did not vary with the width of the plot since there was no variation in surface characteristics between the road and transverse dunes at the ecotone site.

Eq. (1) indicates that the amount of sediment in transport during high wind events varies as a power function of height above the surface. The variation in sediment captured within 2 m of the eroding surface during the 11 sampling periods at our experimental plot is illustrated in Fig. 4. The results indicate a good relationship between height and horizontal mass flux ($R^2 \geqslant 0.9$). Little sediment (3–82 g m^{-1}) was captured by the BSNE collectors at a height of 2 m in the plot while much of the sediment (11,234–201,161 g m^{-1}) in transport was captured within 0.025 m of the surface by the creep collectors (Fig. 4).

Soil loss by creep was 0 g m^{-2} across the 11 sample periods. Soil loss by creep represents the loss of creep-size particles (>0.84 mm) and not loss associated with sediment of varying sizes trapped by the creep collector as portrayed in Fig. 4. The size distribution of sediment trapped by the creep collector is tabulated in Table 3. The sediment trapped by the creep collector was largely composed (76.1%) of particles having a diameter of <0.1 mm whereas no sediment trapped by the creep collector had a diameter >0.84 mm.

Soil loss by either saltation or suspension exceeded loss by creep. Soil loss by saltation or suspension represents the loss of saltation-size (0.84–0.1 mm) or suspension-size (<0.1 mm) particles and not loss associated with sediment of varying sizes trapped by the BSNE collectors as portrayed in Fig. 4. Soil loss by saltation ranged from 4 to 488 g m^{-2} whereas soil loss by suspension ranged from 19 to 1784 g m^{-2} across the 11 sampling periods (Table 2). Saltation constituted 21.6% of the total soil loss, with saltation ranging from 14.2% to 31.1% of the soil loss across all sampling periods. Similarly, suspension constituted 78.4% of the total soil loss, with suspension ranging from 68.9% to 85.8% of the soil loss

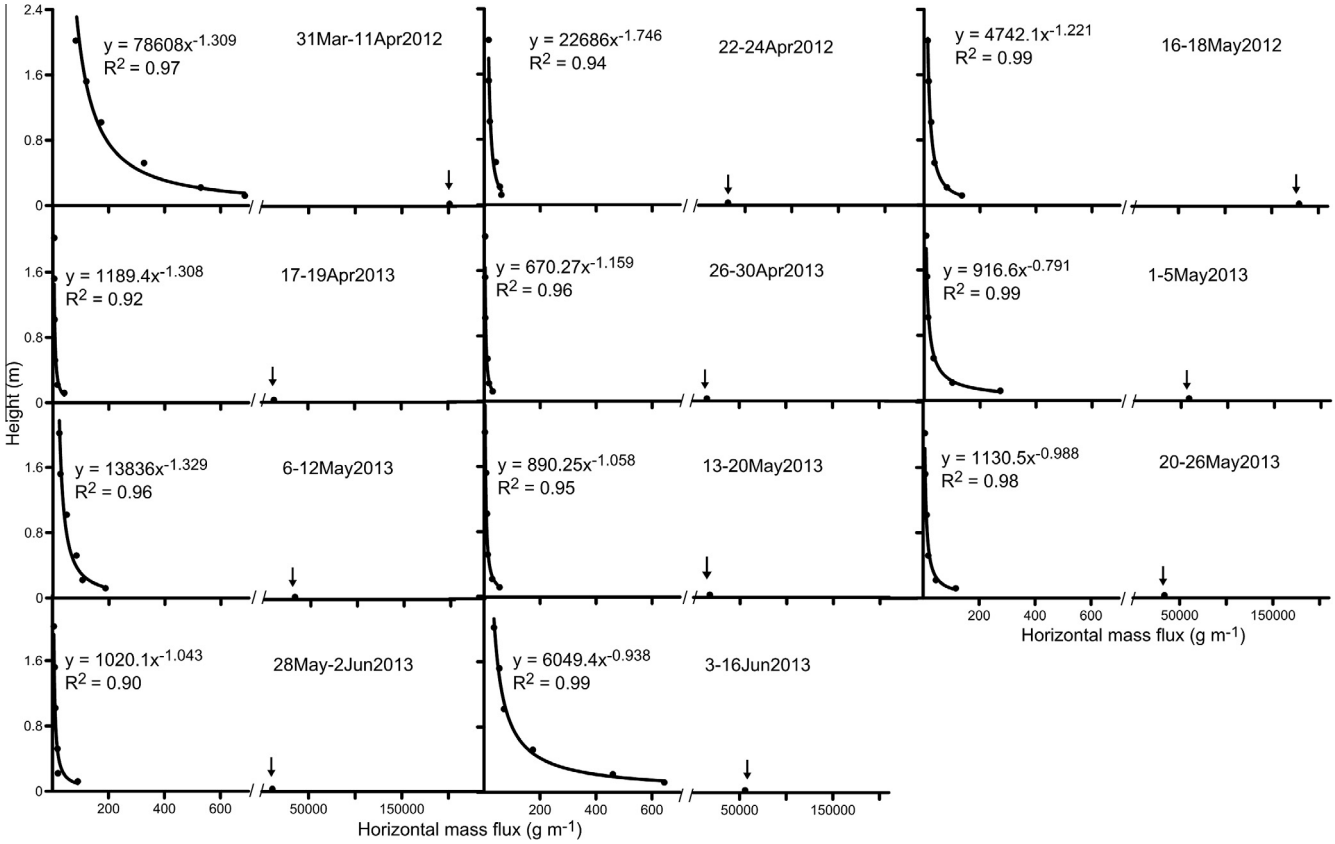

Fig. 4. Horizontal mass flux as a function of height above the eroding surface during 11 high wind events. Sediment was trapped by BSNE collectors positioned at six heights (0.025–2 m) and creep collectors (identified by arrows) positioned at 0–0.025 m.

Table 3
Size distribution of soil trapped by creep collector during 11 sampling periods in 2012 and 2013.

Year	Sampling period[1]	Mass fraction[2] >0.84 mm	0.1–0.84 mm	<0.1 mm
2012	31Mar–11Apr	0	0.219	0.781
	20–24Apr	0	0.201	0.799
	16–18May	0	0.219	0.781
2013	17–19Apr	0	0.255	0.744
	26–30Apr	0	0.335	0.666
	1–5 May	0	0.291	0.709
	6–12May	0	0.222	0.779
	13–20May	0	0.207	0.792
	20–26May	0	0.252	0.749
	28May–2Jun	0	0.253	0.747
	3–16Jun	0	0.172	0.829
Average		0	0.239	0.761

[1] Dates when collectors were installed and retrieved from the experimental site.
[2] Mass fraction is weight of soil within the specified size range divided by total weight of soil trapped by creep collector.

across all sampling periods. Saltation and suspension flux constituted respectively 4.1% and 95.9% of the soil flux measured 0.1 to 2 m above the surface based upon the size distribution of sediment trapped in the BSNE collectors for all 11 sample periods (Table 4). No particles with a diameter >0.84 mm were trapped by the BSNE collectors for all 11 sample periods.

The size distribution of sediment trapped by BSNE collectors changed with height (Table 4). Indeed, the proportion of soil flux moving in saltation decreased with height while that moving in suspension increased with height. The proportion of soil flux moving in saltation was 9.4% at a height of 0.1 m, 5.8% at a height of 0.2 m, 4.5% at a height of 0.5 m, 2.7% at a height of 1 m, and 1.9% at a height of 2 m. In contrast, the proportion of soil flux moving in suspension constituted 90.6% at a height of 0.1 m, 94.2% at a height of 0.2 m, 95.5% at a height of 0.5 m, 97.3% at a height of 1 m, and 98.1% at a height of 2 m. Based upon sediment trapped by creep and BSNE collectors, the relationship between the proportion of soil flux moving in saltation and height was defined as:

$$y = 2.73x^{-0.564} \quad (8)$$

where y is proportion of soil flux moving in saltation and x is height (m). According to this relationship, 85% and 90% of the decrease in soil flux moving in saltation from a height of 0.025 to 2 m occurred respectively at a height of 0.3 and 0.5 m. This range in height of saltation is in agreement with data of Dong and Qian (2007) who reported a saltation height of 0.36 m for sands in the Tengger Desert of China.

3.2. Simulating soil loss using SWEEP

The simulated total soil loss as well as loss associated with creep plus saltation and suspension for the 11 sampling periods is tabulated in Table 2. There was good agreement between the measured and simulated total soil loss as indicated by a high value for d of 0.76 (Table 5). The adequate agreement of the SWEEP in simulating total soil loss was due in part to the good performance of the model in simulating creep plus saltation. Indeed, adequate performance of SWEEP in simulating creep plus saltation was supported by a high value for d as 0.71. Regression analysis ($Y = 1.86X + 0$, $R^2 = 0.63$) and difference of mean (105.6 g m^{-2}) indicated, however, some tendency for SWEEP to overestimate the measured creep plus saltation. No significant differences were evident

Table 4
Size distribution of sand trapped by BSNE collectors during 11 sampling periods in 2012 and 2013.

Year	Sampling period[1]	Particle size range (mm)	Mass fraction at height[2]					
			0.1 m	0.2 m	0.5 m	1 m	1.5 m	2 m
2012	31Mar–11Apr	>0.84	0	0	0	0	0	0
		0.1–0.84	0.082	0.049	0.035	0.027	0.014	0.015
		<0.1	0.918	0.951	0.965	0.973	0.986	0.985
	20–24Apr	>0.84	0	0	0	0	0	0
		0.1–0.84	0.073	0.040	0.036	0.026	0.012	0.012
		<0.1	0.927	0.960	0.964	0.974	0.988	0.988
	16–18May	>0.84	0	0	0	0	0	0
		0.1–0.84	0.091	0.059	0.034	0.028	0.016	0.017
		<0.1	0.909	0.941	0.966	0.972	0.984	0.983
2013	17–19Apr	>0.84	0	0	0	0	0	0
		0.1–0.84	0.039	0.014	0.009	0.005	0.000	0.000
		<0.1	0.961	0.986	0.991	0.995	1.000	1.000
	26–30Apr	>0.84	0	0	0	0	0	0
		0.1–0.84	0.055	0.029	0.079	0.041	0.015	0.017
		<0.1	0.945	0.971	0.921	0.959	0.985	0.983
	1–5May	>0.84	0	0	0	0	0	0
		0.1–0.84	0.143	0.047	0.052	0.049	0.030	0.033
		<0.1	0.857	0.953	0.948	0.951	0.970	0.968
	6–12May	>0.84	0	0	0	0	0	0
		0.1–0.84	0.035	0.017	0.023	0.014	0.011	0.042
		<0.1	0.965	0.983	0.977	0.986	0.989	0.958
	13–20May	>0.84	0	0	0	0	0	0
		0.1–0.84	0.150	0.169	0.026	0.039	0.010	0.012
		<0.1	0.850	0.831	0.974	0.961	0.990	0.988
	20–26May	>0.84	0	0	0	0	0	0
		0.1–0.84	0.021	0.012	0.010	0.013	0.012	0.014
		<0.1	0.979	0.988	0.990	0.987	0.988	0.986
	28May–2Jun	>0.84	0	0	0	0	0	0
		0.1–0.84	0.251	0.081	0.060	0.046	0.028	0.040
		<0.1	0.749	0.920	0.940	0.954	0.972	0.960
	3–16Jun	>0.84	0	0	0	0	0	0
		0.1–0.84	0.094	0.119	0.136	0.004	0.004	0.003
		<0.1	0.906	0.882	0.864	0.996	0.996	0.997

[1] Dates when collectors were installed and retrieved from the experimental site.
[2] BSNE collectors were positioned 0.1, 0.2, 0.5, 1.0, 1.5, and 2.0 m above the surface. Mass fraction is weight of soil within the specified size range divided by total weight of soil trapped by BSNE collector.

Table 5
Statistical comparisons of measured and simulated total soil loss; creep plus saltation, and suspension transport.

Statistic	Total soil loss (g m^{-2})	Creep transport (g m^{-2})	Saltation transport (g m^{-2})	Suspension transport (g m^{-2})	Creep plus saltation transport (g m^{-2})
Paired-samples *t*-test	0.079	0.048	0.115	0.045	0.114
R^2 (intercept≠0)	0.76	–	0.64	0.31	0.64
R^2 (intercept = 0)	0. 76	–	0.63	0.23	0.63
RMSE (g m^{-2})	459.2	18.2	219.5	591.6	220.2
Difference of mean[1] (g m^{-2})	−241.6	−0.4	105.2	−347.3	105.6
Index of agreement (*d*)	0.76	0	0.71	0.43	0.71
Modeling efficiency (EF)	0.47	–	−1.81	−0.41	−1.83

[1] Difference of mean is simulated minus measured value.

between the measured and simulated total soil loss and creep plus saltation based upon the Paired-samples *t*-test.

The SWEEP model inadequately simulated suspension based upon a low *d* (0.43). Regression analysis ($Y = 0.06X + 0$, $R^2 = 0.23$) and negative difference of mean (−347.3 g m^{-2}) suggested that SWEEP underestimated the measured suspension by 94%. The performance of the SWEEP in simulating total soil loss, however, may not have been influenced by the underestimation of suspension because suspension constituted only 13% of the simulated soil loss (Table 2).

Sources of creep and saltation in the SWEEP include surface abrasion of aggregates and direct emission of creep-size and saltation-size particles. We assume, however, that the contribution of abrasion to creep and saltation is minimal in this study due to little aggregation of the aeolian sand. Thus, direct emission of creep-size and saltation-size particles is the primary source of creep and saltation. Adequate simulation of creep plus saltation therefore implies good performance in simulating direct emission of creep-size and saltation-size particles. Sources of suspension in the SWEEP include direct emission of suspension-size particles, surface abrasion of aggregates, and breakdown of creep-size and saltation-size particles. The contribution of the breakdown of creep-size and saltation-size particles to suspension is likely small due to the high stability of aggregates and sand particles (Table 1). Thus, emission of suspension-size particles may be the primary source for suspension. Suspension constituted 79.8% of the measured soil loss, but only comprised 24.7% of the soil (Table 1). This suggests underestimation of suspension may be due to underestimation of the direct emission of suspension-size particles.

Simulation of soil loss by creep plus saltation and suspension as recorded in Table 2 was based on the average wind direction during a sample period. In addition, computation of measured soil loss was also dependent on the average wind direction during the sample period since sediment was collected by integrated, non-recording collectors during multiple high wind events. Simulated soil loss, however, may be influenced by wind direction during separate high wind events within a sample period. Therefore, we simulated soil loss and loss associated with creep plus saltation and suspension based upon wind direction for separate high wind events occurring within a sample period. Similar statistical results were obtained when using the average wind direction or wind direction for separate events during a sampling period. For example, the difference of mean was $-261\ g\ m^{-2}$, d was 0.70, EF was 0.36, and RMSE was $501\ g\ m^{-2}$ when simulating soil loss using wind direction for separate high wind events within a sample period. Likewise, the difference of mean was $88\ g\ m^{-2}$, d was 0.71, EF were −1.33, and RMSE was $200\ g\ m^{-2}$ when simulating creep plus saltation using wind direction for separate high wind events. Lastly, the difference of mean was $-349\ g\ m^{-2}$, d was 0.42, EF was −0.42, and RMSE was $596\ g\ m^{-2}$ when simulating suspension using wind direction for separate high wind events within a sample period.

The performance of the SWEEP was further assessed using alternate values for maximum and minimum aggregate size. Based upon values estimated by the SWEEP (maximum and minimum aggregate size was 1.54 and 0.01 mm), simulated soil loss increased for all erosion events as compared to soil loss reported in Table 2. The simulated soil loss increased by 12% for the 26–30 April 2013 erosion event to 25% for the 20–24 April 2012 erosion event. The increase in simulated soil loss was due to an increase in suspension and not creep plus saltation. While simulated loss due to suspension increased by 32% to 200%, simulated loss due to creep plus saltation decreased by 1% to 13% across all erosion events. The increase in simulated suspension resulted in part from emission of smaller particles associated with the decrease in the minimum aggregate size from 0.05 to 0.01 mm. Model performance in simulating soil loss appeared to improve using estimates of maximum and minimum aggregate size as d was 0.81, EF was 0.55, RMSE was $422\ g\ m^{-2}$, and difference of mean was $-205\ g\ m^{-2}$. Performance in simulating creep plus saltation and suspension also improved using estimates of maximum and minimum aggregate size. For example, model performance statistics for creep plus saltation included d of 0.72, EF of −1.6, RMSE of $213\ g\ m^{-2}$, and difference of mean of $101\ g\ m^{-2}$. For suspension, d was 0.47, EF was −0.2, RMSE was $537\ g\ m^{-2}$, and difference of mean was $-306\ g\ m^{-2}$.

3.3. Simulating potential creep and saltation using SWEEP

Creep and saltation are simulated as a single component in SWEEP because these processes have a limited transport capacity that depends upon friction velocity and surface roughness (Tatarko, 2008). Since SWEEP does not separate creep and saltation and has not been modified to provide such information, we attempted separating these components according to aggregate size. The SWEEP estimates soil loss based upon the aggregate size distribution of the soil, which can be used to estimate the potential fraction of simulated creep, saltation and suspension. The SWEEP uses the GMD and GSD of the aggregate size distribution to determine aggregate sizes <0.01, <0.1, 0.1–0.84, and >0.84 mm in diameter. Based upon a GMD and GSD of respectively 0.254 mm and $2.748\ mm\ mm^{-1}$, the simulated percentage of creep, saltation and suspension in the aeolian sand were respectively 6.0%, 93.8%, and 0.2%. These simulated percentages were used to separate the simulated creep plus saltation. Similarly, the measured aggregate size distribution of the aeolian sand (Fig. 5) was used to separate the simulated creep plus saltation. The measured percentages of creep, saltation and suspension were respectively 0%, 83.3%, and 16.7%. Based on the above two methods to separate the simulated creep plus saltation, the SWEEP model appeared to adequately simulate saltation based upon a high d (0.71) using both the measured and simulated mass percentages of creep, saltation, and suspension. The SWEEP model also adequately simulated creep when using the measured mass percentages of creep and saltation. Since the measured percentage of creep was 0%, the SWEEP simulated no creep. This is in contrast to the SWEEP poorly simulating creep when using the simulated mass percentages of creep and saltation. For example, although no creep was measured during any erosion event, simulated creep ranged from $0.01\ g\ m^{-2}$ for the 26–30 April 2013 event to $1.69\ g\ m^{-2}$ for the 31 March–11 April 2012 event.

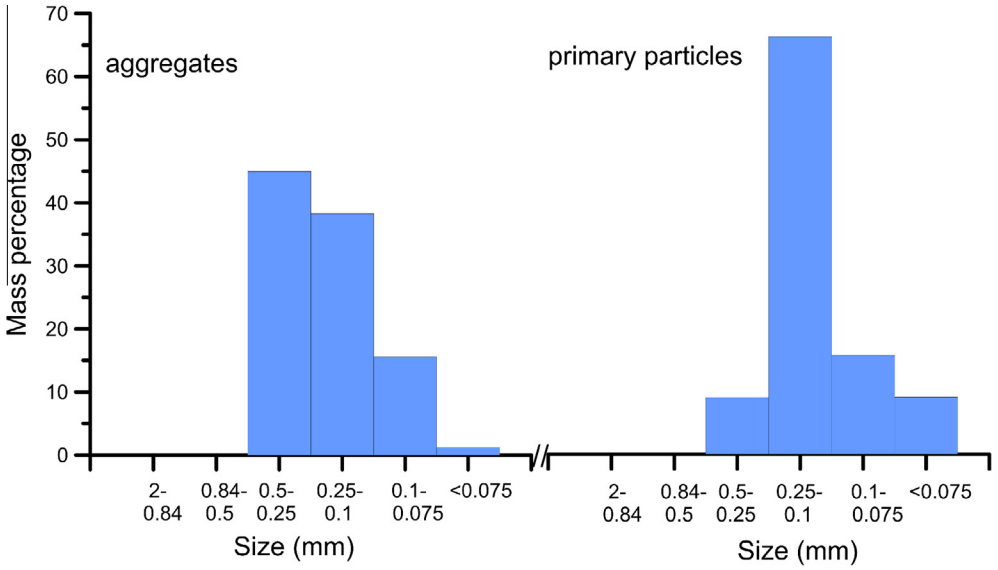

Fig. 5. Aggregate and primary particle size distributions for the Aeolian sand at the experimental site. Aggregate and particle size distributions were determined using respectively a horizontal sieve apparatus and Mastersizer laser diffraction instrument.

4. Conclusion

The ability of SWEEP to simulate creep, saltation, and suspension was tested in a desert–oasis ecotone within the Tarim Basin. The SWEEP adequately simulated total soil loss and loss due to creep plus saltation. However, the model appeared to underestimate loss due to suspension. Total soil loss was not influenced by underestimation of suspension because of the relatively small proportion (13%) of suspension in simulated total sediment loss. Creep and saltation are simulated as a single transport component in SWEEP because these processes have limited transport capacity. Aggregate size distribution of the aeolian sand was used, however, to separate creep and saltation. The SWEEP simulated creep and saltation adequately, but only when the measured aggregate size distribution was used to ascertain the percentage of creep-size and saltation-size particles.

Acknowledgements

The authors are grateful to Dr. Lawrence Hagen (retired) at the USDA–ARS Wind Erosion Research Unit in Manhattan, KS and Dr. Larry Wagner at the USDA–ARS Agricultural Systems Research Unit in Ft. Collins, CO, for their assistance with the application of SWEEP. This research was supported by National Natural Science Foundation of China (Grant No. 41171019), One Hundred Talented Researchers Program of Chinese Academy of Sciences, the Special Major Science and Technology Projects in Xinjiang Uygur Autonomous Region (201130106-1) and West Light Foundation of the Chinese Academy of Sciences (XBBS201104).

References

Allmaras, R.R., Burwell, R.E., Larson, W.E., 1966. Total porosity and random roughness of the interrow zones influenced by tillage. US Department of Agriculture Conservation Research Report 7.

Armbrust, D.V., 1984. Wind and sandblast injury to field crops: effect of plant age. Agron. J. 76, 991–993.

Bagnold, R.A., 1941. The Physics of Blown Sand and Desert Dunes. William Morrow & Company, New York, NY.

Buschiazzo, D.E., Zobeck, T.M., 2008. Validation of WEQ, RWEQ and WEPS wind erosion for different arable land management systems in the Argentinean Pampas. Earth Surf. Proc. Land. 33, 1839–1850.

Chan, Y.C., McTainsh, G.H., Leys, J.F., McGowan, H.A., Tews, E.K., 2005. Influence of the 23 October 2002 dust storm on the air quality of four Australian cities. Water Air Soil Pollut. 164, 329–348.

Chepil, W.S., 1945. Dynamics of wind erosion: I. Nature of movement of soil by wind. Soil Sci. 60, 305–320.

Currence, H.D., Lovely, W.G., 1970. The analysis of soil surface roughness. Trans. Am. Soc. Agric. Eng. 13, 710–714.

Dong, Z., Liu, X., Wang, H., Zhao, A., Wang, X., 2002. The flux profile of a blowing sand cloud: a wind tunnel investigation. Geomorphology 49, 219–230.

Dong, Z., Qian, G., 2007. Characterizing the height profile of the flux of wind-eroded sediment. Environ. Geol. 51, 835–845.

Feng, G., Sharratt, B., 2009. Evaluation of the SWEEP model during high winds on the Columbia Plateau. Earth Surf. Proc. Land. 34, 1461–1468.

Fryrear, D.W., 1986. A field dust sampler. J. Soil Water Conserv. 41, 117–120.

Fryrear, D.W., Stout, J.E., Hagen, L.J., Vories, E.D., 1991. Wind erosion: field measurement and analysis. Trans. Am. Soc. Agric. Eng. 34, 155–160.

Funk, R., Skidmore, E.L., Hagen, L.J., 2004. Comparison of wind erosion measurements in Germany with simulated soil losses by WEPS. Environ. Model. Software 19, 177–183.

Gardner, W.R., 1956. Representation of soil aggregate-size distribution by a logarithmic-normal distribution. Soil Sci. Soc. Am. Proc. 20, 151–153.

Goossens, D., Offer, Z., London, G., 2000. Wind tunnel and field calibration of five Aeolian sand traps. Geomorphology 35, 233–252.

Hagen, L.J., 1991. A wind erosion prediction system to meet user needs. J. Soil Water Conserv. 46, 106–111.

Hagen, L.J., Wagner, L.E., Tatarko, J., Skidmore, E.L., Durar, A.A., Steiner, L.J., Schomberg, H.H., Retta, A., Armbrust, D.V., Zobeck, T.M., Unger, P.W., Ding, D., Elminyawi, I., 1995. Wind erosion prediction system: technical description. In: Proceeding of the WEPP/WEPS Symposium. Soil and Water Conservation Society, Des Moines, IA.

Hagen, L.J., 1997. Wind erosion prediction system: erosion submodel. In: Skidmore, E.L., Tatarko, J., (Eds.), Wind Erosion – Proceedings of an International Symposium/Workshop, 3–5 June 1997, Manhattan, Kansas. USDA-Agricultural Research Service, Wind Erosion Research Unit and Kansas State University. Available at: <https://infosys.ars.usda.gov/WindErosion/symposium/abstracts/hagen.htm>.

Hagen, L.J., Wagner, L.E., Skidmore, E.L., 1999. Analytical solutions and sensitivity analysis for sediment transport in WEPS. Trans. Am. Soc. Agric. Eng. 42, 1715–1721.

Hagen, L.J., 2004a. Fine particulates (PM10 and PM 2.5) generated by breakage of mobile aggregates during simulated wind erosion. Trans. Am. Soc. Agric. Eng. 47, 107–112.

Hagen, L.J., 2004b. Evaluation of the Wind Erosion Prediction System (WEPS) erosion submodel on cropland fields. Environ. Model. Software 19, 171–176.

Hagen, L.J., Van Pelt, R.S., Sharratt, B.S., 2010. Estimating the saltation and suspension components from field wind erosion. Aeolian Res. 1, 147–153.

Hagen, L.J., 2010. Erosion by wind: modeling. In: Lal, R. (Ed.), Encyclopedia of Soil Science, second ed. Taylor and Francis, London, pp. 1–4, New York, NY.

Honda, M., Shimizu, H., 1998. Geochemical, mineralogical and sedimentological studies on the Taklimakan Desert sands. Sedimentology 45, 1125–1143.

Li, X., Feng, G., Sharratt, B., Zheng, Z., 2015. Aerodynamic properties of agricultural and natural surfaces in northwestern Tarim Basin. Agric. For. Meteorol. 204, 37–45.

Loague, K., Green, R.E., 1991. Statistical and graphical methods for evaluating solute transport models: overview and application. J. Contam. Hydrol. 7, 51–73.

Lyles, L., 1977. Wind erosion: processes and effect on soil productivity. Trans. Am. Soc. Agric. Eng. 20, 880–884.

Ma, L., Ahuja, L.R., Saseendran, S.A., Malone, R.W., Green, T.R., Nolan, B.T., Bartling, P. N.S., Flerchinger, G.N., Boote, K.J., Hoogenboom, G., 2011. A protocol for parameterization and calibration of RZWQM2 in field research. In: Ahuja, L., Ma, L. (Eds.), Methods of introducing system models into agricultural research. Advances in agricultural systems modeling 2. Transdisciplinary research, synthesis, and applications. American Society of Agronomy, Madison, WI, pp. 1–64.

Maurer, T., Gerke, H.H., 2011. Modelling Aeolian sediment transport during initial soil development on an artificial catchment using WEPS and aerial images. Soil Tillage Res. 117, 148–162.

McDonald, J.H., 2008. Handbook of Biological Statistics. Sparky House Publishing, Baltimore, MD, pp. 176–180.

Mendez, M.J., Funk, R., Buschiazzo, D.E., 2011. Field wind erosion measurements with big spring number eight (BSNE) and modified Wilson and Cook (MWAC) samplers. Geomorphology 129, 43–48.

Mikami, M., Yamada, Y., Ishizuka, M., Ishimaru, T., Gao, W., Zeng, F., 2005. Measurement of saltation process over Gobi and sand dunes in the Taklimakan Desert, China, with newly developed sand particle counter. In: J. Geophys. Res. 110. http://dx.doi.org/10.1029/2004JD004688, D18S02.

Namikas, S.L., 2003. Field measurement and numerical modeling of Aeolian mass flux distributions on a sandy beach. Sedimentology 50, 303–326.

Rotnicka, J., 2013. Aeolian vertical mass flux profiles above dry and moist soil beach surfaces. Geomorphology 187, 27–37.

Saleh, A., Fryrear, D.W., 1995. Threshold wind velocities of wet soils as affected by windblown soil. Soil Sci. 160, 304–309.

Shao, Y., 2000. Physics and Modelling of Wind Erosion. Kluwer Academic Publishers, Dordrecht, The Netherlands.

Shao, Y., Lu, H., 2000. A simple expression for wind erosion threshold friction velocity. J. Geophys. Res. 105, 22437–22443.

Sharratt, B., 2011. Size distribution of windblown sediment emitted from agricultural fields in the Columbia Plateau. Soil Sci. Soc. Am. J. 75, 1054–1060.

Sharratt, B.S., Lauer, D., 2006. Particulate matter concentration and air quality affected by windblown dust in the Columbia Plateau. J. Environ. Qual. 35, 2011–2016.

Sharratt, B., Feng, G., Wendling, L., 2007. Loss of soil and PM10 from agricultural fields associated with high winds on the Columbia Plateau. Earth Surf. Proc. Land. 32, 621–630.

Sharratt, B.S., Feng, G., 2009. Windblown dust influenced by conventional and undercutter tillage within the Columbia Plateau, USA. Earth Surf. Proc. Land. 34, 1323–1332.

Sharratt, B., Edgar, R., 2011. Implications of changing PM10 air quality standards on Pacific Northwest communities affected by windblown dust. Atmos. Environ. 45, 4626–4630.

Sharratt, B.S., Vaddella, V., Feng, G., 2013. Threshold friction velocity influenced by wetness of soils within the Columbia Plateau. Aeolian Res. 9, 175–182.

Su, Y.Z., Zhao, W.Z., Su, P.X., Zhang, Z.H., Wang, T., Ram, R., 2007. Ecological effects of desertification control and desertified land reclamation in an oasis–desert ecotone in an arid region: a case study in Hexi Corridor, northwest China. Ecol. Eng. 29, 117–124.

Tatarko, J., 2008. Single-event wind erosion evaluation program: SWEEP user manual draft. USDA-ARS wind erosion research unit. 45pp. Available at: <http://www.ars.usda.gov/services/software/download.htm?softwareid=415>.

Tatarko J., 2010. The wind erosion prediction system: WEPS 1.0 user manual. Available at: <https://infosys.ars.usda.gov/WindErosion/weps/wepshome.html>.

Tchakerian, V.P., 1999. Stone pavement. In: Mares, M.A. (Ed.), Encyclopedia of Deserts. University of Oklahoma Press, Norman, OK, pp. 542–543.

Van Donk, S.J., Huang, X., Skidmore, E.L., Anderson, A.B., Gebhart, D.L., Prehoda, V.E., Kellog, E.M., 2003. Wind erosion from military training lands on the Mojave Desert, California, U.S.A. J. Arid Environ. 54, 687–703.

Visser, S.M., Sterk, G., Karssenberg, D., 2005. Wind erosion modeling in a Sahelian environment. Environ. Model. Software 20, 69–84.

Wagner, L.E., 2013. A history of wind erosion prediction models in the United States Department of Agriculture: the Wind Erosion Prediction System (WEPS). Aeolian Res. 10, 9–24.
Wang, Z., Zheng, X., 2004. Theoretical prediction of creep flux in Aeolian sand transport. Powder Technol. 139, 123–128.
Wang, X., Dong, Z., Zhang, J., Qu, J., Zhao, A., 2003. Grain size characteristics of dune sands in the central Taklimakan sand sea. Sediment. Geol. 161, 1–14.
Wang, X., Jiang, J., Lei, J., Zhao, C., 2004. Relationship between ephemeral plants distribution and soil moisture on longitudinal dune surface in Gurbantonggut desert. Chin. J. Appl. Ecol. 15, 556–560.
Willmott, C.J., 1981. On the validation of models. Phys. Geogr. 2, 184–194.
Willetts, B.B., Rice, M.A., 1985. Wind tunnel tracer experiments using dyed sand. In: Proceedings of the International Workshop on the Physics of Blown Sand. Department of Theoretical Statistics, Institute of Mathematics, Aarhus University, pp. 225–242.
Zhang, Y., Wang, Y., Jia, P., 2014. Investigation of the statistical features of sand creep motion with wind tunnel experiment. Aeolian Res. 12, 1–7.
Zobeck, T.M., Fryrear, D.W., 1986. Chemical and physical characteristics of windblown sediment I. Quantities and physical characteristics. Trans. Am. Soc. Agric. Eng. 29, 1032–1036.